



# Parametric study of heat-transfer design on the thermoelectric generator system<sup>☆</sup>



Sheng-Chung Tzeng<sup>\*</sup>, Tzer-Ming Jeng, Yi-Liang Lin

Department of Mechanical Engineering, Chienkuo Technology University, Taiwan, ROC

## ARTICLE INFO

Available online 16 January 2014

### Keywords:

Thermoelectric generator  
Heat transfer  
Heat absorber  
Heat sink  
Heat-transfer parameters

## ABSTRACT

This study developed an integral thermoelectric generator system with high-performance heat transfer and thermoelectric conversion functions, using the metal pin-fin array coupling with the forced convection heat transfer technique to be the heat absorber and heat sink. A one-dimensional steady heat conduction model with internal Joule heat generation and Seebeck effect was proposed to predict the power generation performance of the present thermoelectric system including the heat absorber and heat sink at various operation conditions. Critical heat-transfer parameters on the design of the integral thermoelectric generator system were derived and discussed. Finally, a series of systematical experiments were performed to simulate an integral thermoelectric generator system operating at the exhaust pipe. The experimental results also demonstrated the validity of the proposed theoretical model.

Crown Copyright © 2014 Published by Elsevier Ltd. All rights reserved.

## 1. Introduction

Approximately 30% of the energy generated by the combustion of fuel in the engine cylinder will be converted by the cylinder piston motion into the brake force of vehicles (5% of it will be neutralized by friction loss of machine members). In addition, about 70% of it cannot be converted into mechanical energy, but disperses to the environment as waste heat. About a half of the useless heat is emitted with exhaust gas out of the engine, and the other half is emitted by the cooling system of the engine body. If these waste heat can be recovered, the power loss can be reduced, and the thermal pollution to the environment resulted from the waste heat can be also reduced. Some conceptual heat recovery technologies applied on the automotive engine have been introduced briefly by Talom and Beyene [1]. Among these conceptual heat recovery technologies, the thermoelectric generator (TEG) may offer thermoelectric energy conversion in a simple, quiet, reliable and environmentally friendly way. Therefore, there has been a growing interest in the generation technology of TEG and its reverse application (i.e. thermoelectric cooler, TEC) [2–8].

Many studies have investigated the characteristics of thermoelectric generator components and the application of waste heat recovery, showing the importance of waste heat recovery power generation in green energy development. Recently, Chen et al. [9] proposed a three-dimensional thermoelectric generator model and implemented the numerical simulation by a commercial soft (FLUENT). Because the temperature of the industrial heat source usually ranges from hundreds to

more than one thousand degrees, their model accounts for all temperature dependent characteristics of the materials. Consequently, a numerical approximation is used to solve the mathematic equations. They indicated that their model is validated by simulation data from other models and experimental data; it can be used to predict and optimize the system performance of real thermoelectric devices. Sandoz-Rosado et al. [10] implemented a systematic assessment of validity of the standard model which uses an averaged Seebeck coefficient and neglects the non-linear Thomson effect to develop a closed-form solution of the governing heat equation. They proved that the standard model using the integral-averaged Seebeck coefficient (but neglects the Thompson term in the temperature field evaluation) is sufficiently accurate for the thermoelectric system modeling and optimization as an alternative to computationally expensive numerical simulations. Rezanian [11] experimentally investigated the effect of using a specified microchannel heat sink on the power generated by the thermoelectric generator (TEG) system. Their results showed that there was a unique coolant flow rate at any temperature difference of the hot and cold sides of the TEG ( $\Delta T_{\text{teg,av}}$ ) that made maximum net-power, and the value of the optimum flow rate increased when the  $\Delta T_{\text{teg,av}}$  increased.

Most of the previous studies focused on the relationship of the generating electricity and the temperature difference between the cold and hot end surfaces of thermoelectric generator. The studies about critical heat-transfer parameters on the design of the integral thermoelectric system including the heat absorber and heat sink at various operation conditions are few. Therefore, this study developed a platform with high-performance heat transfer and thermoelectric conversion functions, using the metal pin-fin array coupling with the forced convection heat transfer technique to be the heat absorber and heat sink. By using the theoretical model and experimental method, heat transfer and thermoelectric conversion principles were applied to discuss the influences

<sup>☆</sup> Communicated by W.J. Minkowycz.

<sup>\*</sup> Corresponding author at: Department of Mechanical Engineering, Chienkuo Technology University, No. 1, Chieh Shou N Rd., Chang Hua 500, Taiwan, ROC.  
E-mail address: [tsc@ctu.edu.tw](mailto:tsc@ctu.edu.tw) (S.-C. Tzeng).

### Nomenclature

$A$	area ( $\text{m}^2$ )
$F$	flow rates ( $\text{m}^3/\text{h}$ )
$h$	heat transfer coefficient ( $\text{W}/\text{m}^2/\text{K}$ )
$I$	generating current (I)
$k$	thermal conductivity ( $\text{W}/\text{m}/\text{K}$ )
$P$	overall generating electricity (W)
$\dot{q}$	the rate of heat internally generated per unit volume ( $\text{W}/\text{m}^3$ )
$Q$	thermal power (W)
$R$	electric resistance of the variable load ( $\Omega$ )
$R_{\text{int}}$	internal electric resistance ( $\Omega$ )
$T$	temperature ( $^{\circ}\text{C}$ )
$V$	generating voltage (V)

### Greek symbols

$\alpha$	Seebeck coefficient difference (V/K)
$\alpha^*$	Seebeck parameter of TEG (1/K)
$\gamma$	heat-transfer ratio of heat absorber to heat sink
$\delta$	thickness of thermoelectric generator (m)
$\lambda$	Biot number of TEG

### Subscripts

1	the side of heat absorber
2	the side of external heat sink
C	cooling air or cold side of TEG
H	hot air or hot side of TEG
i	at the channel inlet
$i,s$	inner spreader, i.e. the spreader of heat absorber
j	jet cooling air
max	maximum
$o,s$	outer spreader, i.e. the spreader of external heat sink
tg	thermal grease
TEG	thermoelectric generator

of different operation conditions on the energy output of thermoelectric generator and derive the relevant critical heat-transfer parameters, in order to be reference for next physical product of the thermoelectric generator system.

## 2. Experiments and theoretical analysis

### 2.1. Experimental equipments for thermoelectric conversion system

In order to simulate an integral thermoelectric conversion system operating at the exhaust pipe, we built an experimental system shown in Fig. 1(a). The experimental equipment is consisted of (1) hot air supply source; (2) test section; (3) inner heat absorber; (4) thermoelectric generators; (5) external heat sink and (6) data acquisition equipment.

The air source for the experimental system is generated by 10-HP air compressor and stored in 800 L air tank to reduce the impulse. When the rated pressure is reached, the air flows through the oil filter and the dryer to filter the vapor, oil and foreign particles. The air flow rate is adjusted by the SIN-DP electronic flow controller. Before the air enters the test section, it will pass through a high-temperature heater. This heater can heat the air to the rated temperature within a short period of time, and then the hot air is forwarded into the test section. The decomposition chart of the test section is shown in Fig. 1(b). The test section, with a cross section of 80 mm  $\times$  38.5 mm, is made of 40 mm-thick Bakelite with low thermal conductivity to reduce the heat loss dissipated from the walls. In the inside of the test section, a 5 mm-thick stainless

steel is welded to protect the Bakelite against the very hot air. Besides, there are three configurations of heat absorbers that will be installed respectively into the test section: (1) the smooth plate (Mode A); (2) the staggered circular pin-fin array (Mode B) and (3) the inline circular pin-fin array (Mode C). They are all made of aluminum alloy (T6061). There is a thermocouple (TT-T-30SLE) at the inlet of test section to measure the inlet temperature of hot air. The thermocouples are also embedded in the spreader of the heat absorber to measure the relevant temperatures. All the configurations and dimensions of the heat absorbers are shown in Fig. 2(a). Table 1 shows the specifications of the thermoelectric generator made by Russia KRYOTHERM. The thermoelectric generator uses the temperature difference between both sides of the chip module to convert the heat energy into electric energy. This experiment used the thermal grease with high thermal conductivity to affix the hot sides of four thermoelectric generators to the heat absorber, so as to transfer the heat energy of hot air to the thermoelectric generators. The other sides (cold sides) of the thermoelectric generators were affixed to the external heat sink for cooling. The temperature difference between the cold and hot sides of thermoelectric generators increases with the heat-transfer rate, so that a better heat-transfer design will obtain higher generating electricity. In order to obtain the temperatures of cold and hot sides of thermoelectric generators accurately, the spreaders of the heat absorber and heat sink were machined to make some small holes enough for thermocouples to pass through, and then the thermocouples could contact directly to the both sides of the thermoelectric generators. When the thermocouples were embedded into the spreaders, the gaps of the machined holes were filled up with the high-thermal-conductivity thermal grease, so as to reduce the effect of the machined holes for embedding thermocouples on the thermal conduction performances of the heat absorber and heat sink. The external heat sink, fixed to the cold sides of thermoelectric generators for forced convective cooling, was made of aluminum alloy (T6061) with staggered circular pin fins. The configuration and dimension of the heat sink is shown in Fig. 2(b). It used a 1/2-HP blower to feed cooling air in the vertical pipe in diameter of 75 mm, and the inverter controlled the rotational speed of the blower motor to adjust the cooling air rate. The outlet of the vertical pipe was connected to the heat sink, so that the cooling air impacted the pin fins directly for heat exchange. There was additional thermocouple for measuring the jet cooling air temperature. The multifunctional data recorder (YOKOGAWA, MX-100) captured the temperatures ( $T_i$ ,  $T_j$ ,  $T_{i,s}$ ,  $T_{o,s}$ ) of the inlet hot air, jet cooling air, cold and hot sides of the thermoelectric generators. The generating voltage ( $V$ ), the electric resistance of the variable load ( $R$ ), the hot and cooling air flow rates ( $F_H$ ,  $F_C$ ) were also recorded. The computer recorded and integrated all the data. All the data were captured when the temperatures reached thermal balance, namely, the temperature change did not exceed 0.2  $^{\circ}\text{C}$  within 15 min.

### 2.2. Theoretical model for generating electricity and heat transfer mechanism

Fig. 3 is the schematic diagram of the heat transfer mechanism of thermoelectric conversion platform of this study and the relevant thermal network. The compressed air is heated by a heater and the flow rate is adjusted by a flow controller, so as to simulate the temperature and flow rate of the exhaust emitted by the automobile engine. As shown in the figure, the hot air with  $T_i$  temperature enters the inlet end of the thermoelectric conversion platform. The waste heat energy is led to the heat absorber with  $T_{i,s}$  temperature by heat convection with  $h_1$  heat transfer coefficient, the internal heat sink absorbs some of the waste heat energy, and the thermal grease with  $k_{\text{tg}}$  thermal conductivity leads the heat to the hot side of the thermoelectric generator (TEG) with  $T_{\text{TEG},H}$  temperature. Following this, the heat is transferred across the thermoelectric generator by heat conduction with  $k_{\text{TEG}}$  thermal conductivity to the cold side of the thermoelectric generator with  $T_{\text{TEG},C}$  temperature. The thermal grease with  $k_{\text{tg}}$  thermal conductivity leads the heat to the spreader of the external heat sink with  $T_{o,s}$  temperature,

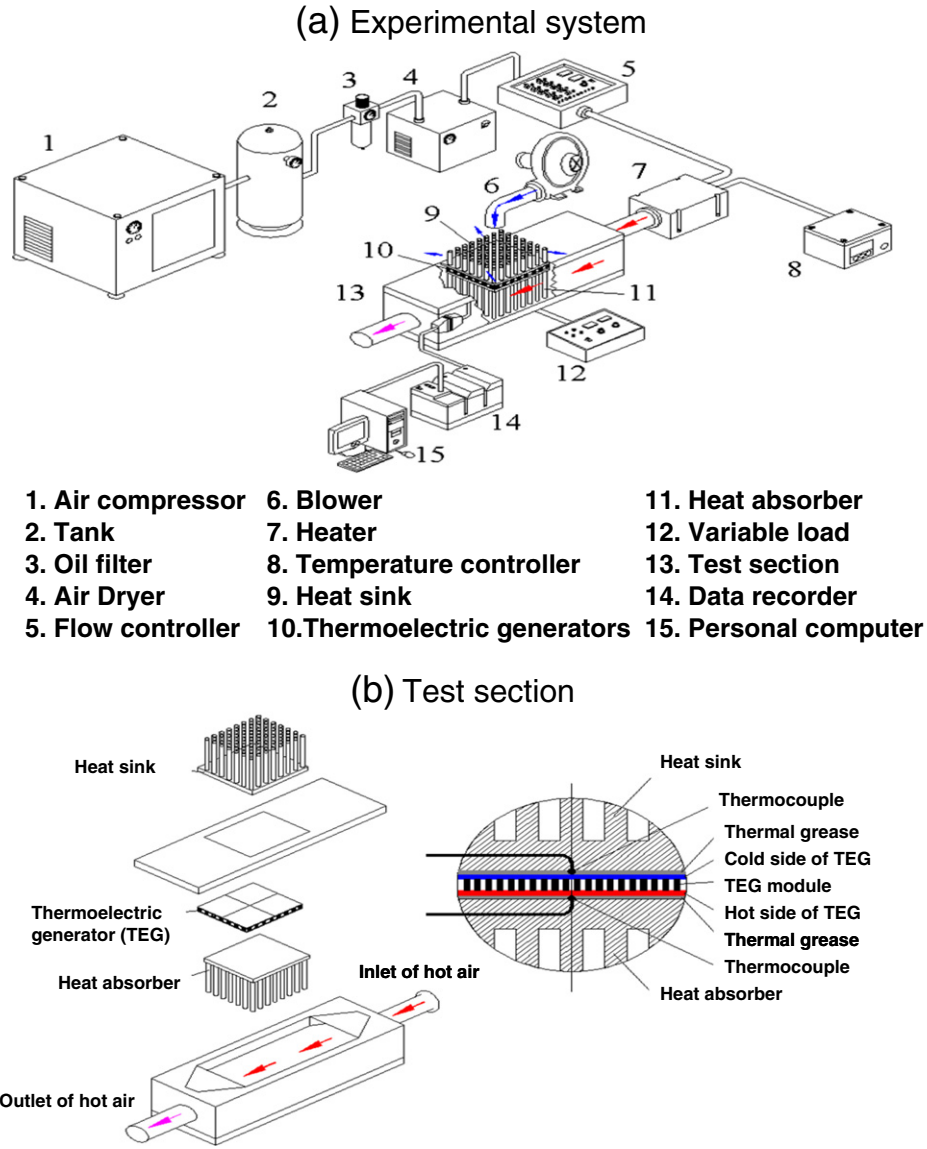


Fig. 1. Schematic diagram of experimental system and decomposition chart of test section.

and then the external heat sink uses the forced convective impinging cooling with  $h_2$  heat transfer coefficient to emit heat to the external environment by the jet air flow with  $T_j$  temperature. The heat collection and heat dissipation separately at the hot and cold sides of the thermoelectric generator make the temperature difference between the both sides of the thermoelectric generator to generate electricity due to Seebeck effect. At the same time, the internal Joule heating will happen in the thermoelectric generator due to the  $R_{int}$  internal electric resistance. It needs to be noted that as the thickness of thermal grease layer is very thin and the  $k_{tg}$  thermal conductivity is quit high, the  $T_{i,s}$  and  $T_{o,s}$  measured in the experiment almost equal  $T_{TEG,H}$  and  $T_{TEG,C}$  respectively and the combined thermal conductivity of thermal grease layers and thermoelectric generators are almost equivalent to  $k_{TEG}$ .

The heat transferred across the thermoelectric generator can be modeled by the one-dimensional steady heat conduction equation for solids with internal energy generation [12], which is written as:

$$\frac{\partial^2 T}{\partial x^2} + \frac{\dot{q}}{k_{TEG}} = 0 \quad (1)$$

where  $\dot{q}(= R_{int} I^2 / \delta / A_{TEG})$  is the rate of heat internally generated per unit volume while  $I$  and  $\delta$  are the generating current and the

thickness of thermoelectric generator, respectively. Assuming the constant temperatures at the hot and cold sides as boundary conditions:

$$T(0) = T_{i,s} \quad \text{at } x = 0 \quad (2)$$

$$T(\delta) = T_{o,s} \quad \text{at } x = d \quad (3)$$

Eqs. (1)–(3) can be solved as:

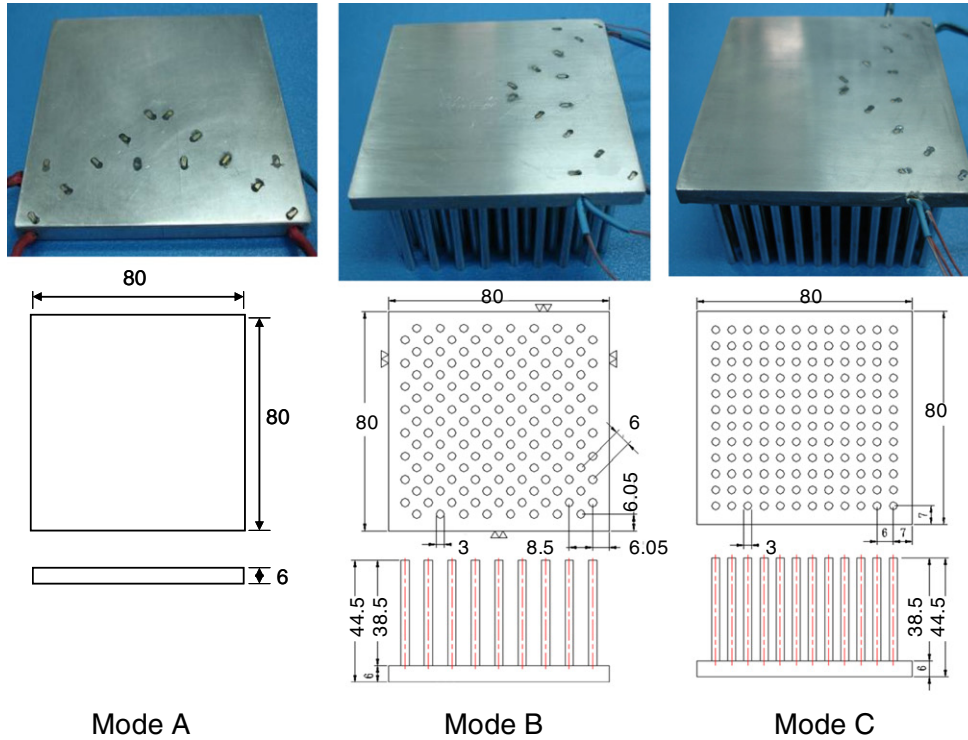
$$T(x) = T_{i,s} - \frac{\dot{q}}{2k_{TEG}} x^2 + \frac{T_{o,s} - T_{i,s} + \dot{q} \delta^2 / 2k}{\delta} x. \quad (4)$$

By considering the Seebeck effect at the hot and cold sides, the thermal power input to the hot side ( $Q_H$ ) and the thermal power output from the cold side ( $Q_C$ ) are separately given by

$$Q_H = \frac{k_{TEG} A_{TEG}}{\delta} (T_{i,s} - T_{o,s}) + \alpha T_{i,s} I - \frac{1}{2} R_{int} I^2 \quad (5)$$

$$Q_C = \frac{k_{TEG} A_{TEG}}{\delta} (T_{i,s} - T_{o,s}) + \alpha T_{o,s} I + \frac{1}{2} R_{int} I^2 \quad (6)$$

## (a) Inner heat absorbers



## (b) External heat sink

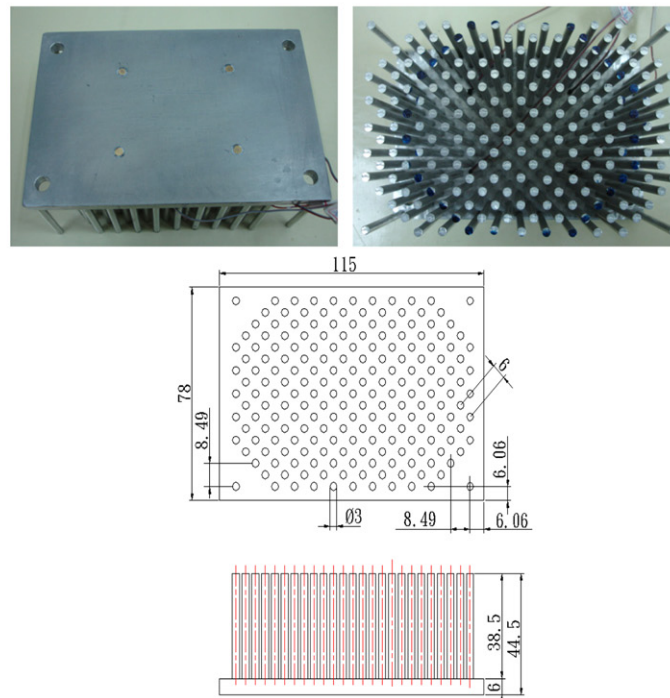


Fig. 2. Configurations and dimensions of heat absorbers and heat sink (unit: mm).

where  $A_{TEG}$  represents the area of the thermoelectric generator and  $\alpha$  is the Seebeck coefficient difference. Eqs. (1)–(6) are often shown in the previous papers about the thermoelectric generator. However, a one-dimensional steady heat conduction model with internal Joule heat generation and Seebeck effect, which can predict the power generation performance of the present thermoelectric system including the heat

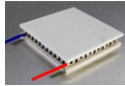
absorber and heat sink at various operation conditions, is not reported. The relevant governing energy equation is still like as Eq. (1), but the corresponding boundary conditions are changed as follows:

$$h_1 A_1 (T_i - T_{i,s}) = -k_{TEG} A_{TEG} \frac{\partial T}{\partial x} \Big|_{x=0} \quad \text{at } x = 0 \quad (7)$$

**Table 1**

Specifications of the present thermoelectric generator module (model: TGM-287-1.0-1.5, Russia KRYOTHERM).

Dimensions: 40 mm × 40 mm × 3.8 mm



Temperature at cold side: 50 °C/temperature at hot side: 150 °C

Generating voltage	Generating current	Generating power	Generating efficiency
4.77 (V)	0.47 (A)	2.23 (W)	2.7 (%)
Electric resistance (Ω)	Thermal resistance (°C/W)		
10.2	1.16		

Temperature at cold side: 100 °C/temperature at hot side: 200 °C

Generating voltage	Generating current	Generating power	Generating efficiency
4.52 (V)	0.43 (A)	1.93 (W)	2.3 (%)
Electric resistance (Ω)	Thermal resistance (°C/W)		
10.6	1.13		

$$h_2 A_2 (T_{o,s} - T_j) = -k_{TEG} A_{TEG} \frac{\partial T}{\partial x} \Big|_{x=\delta} \quad \text{at } x = d \quad (8)$$

Eqs. (1), (7) and (8) can be also solved as Eq. (4), as well as the temperatures at the hot and cold sides ( $T_{o,s}$  and  $T_{i,s}$ ) are separately given by

$$T_{i,s} = \frac{\left( \frac{\delta A_{TEG}}{h_2 A_2} + \frac{\delta^2}{2k_{TEG}} \right) \dot{q} + \left( \frac{h_1 A_1}{h_2 A_2} + \frac{h_1 A_1 \delta}{k_{TEG} A_{TEG}} \right) T_i + T_j}{\frac{h_1 A_1}{h_2 A_2} + \frac{h_1 A_1 \delta}{k_{TEG} A_{TEG}} + 1} \quad (9)$$

$$T_{o,s} = -\frac{h_1 A_1}{h_2 A_2} T_{i,s} + \frac{\delta A_{TEG}}{h_2 A_2} \dot{q} + \frac{h_1 A_1}{h_2 A_2} T_i + T_j. \quad (10)$$

Then, taking into account the Seebeck effect at the hot and cold sides, the  $Q_H$  and  $Q_C$  are separately given by

$$Q_H = h_1 A_1 (T_{i,s} - T_{o,s}) + \alpha T_{i,s} I \quad (11)$$

$$\begin{aligned} Q_C &= -k_{TEG} A_{TEG} \frac{\partial T}{\partial x} \Big|_{x=\delta} + \alpha T_{o,s} I \\ &= h_1 A_1 (T_{i,s} - T_{o,s}) + \delta A_{TEG} \dot{q} + \alpha T_{o,s} I. \end{aligned} \quad (12)$$

Therefore, the overall generating electricity ( $P$ ) can be written as follows:

$$\begin{aligned} P &= Q_H - Q_C \\ &= \alpha I (T_{i,s} - T_{o,s}) - R_{int} I^2. \end{aligned} \quad (13)$$

If the generating current ( $I$ ) equals  $\alpha(T_{i,s} - T_{o,s})/2R_{int}$ , it will have the maximum generating electricity  $P_{max} = \alpha^2(T_{i,s} - T_{o,s})^2/4R_{int}$ . At the same time, the generating voltage ( $V$ ) is written as  $\alpha(T_{i,s} - T_{o,s})/2$ . Following this, we introduce some critical thermal parameters such as

$$\gamma = \frac{h_1 A_1}{h_2 A_2}, \lambda = \frac{h_1 A_1 \delta}{k_{TEG} A_{TEG}}, \alpha^* = \frac{\alpha^2 \delta}{4k_{TEG} A_{TEG} R_{int}}. \quad (14)$$

Then, substituting  $\dot{q} = RI/\delta/A_{TEG}$ ,  $I = \alpha(T_{i,s} - T_{o,s})/2R_{int}$  and Eq. (14) into Eqs. (9) and (10), one can obtain the temperature difference ( $T_{i,s} - T_{o,s}$ ) to have the maximum generating electricity  $P_{max} (= \alpha^2(T_{i,s} - T_{o,s})^2/4R_{int})$ .

$$\alpha^* (T_{i,s} - T_{o,s})^2 - (\gamma + \lambda + 1) (T_{i,s} - T_{o,s}) + \lambda (T_i - T_j) = 0 \quad (15)$$

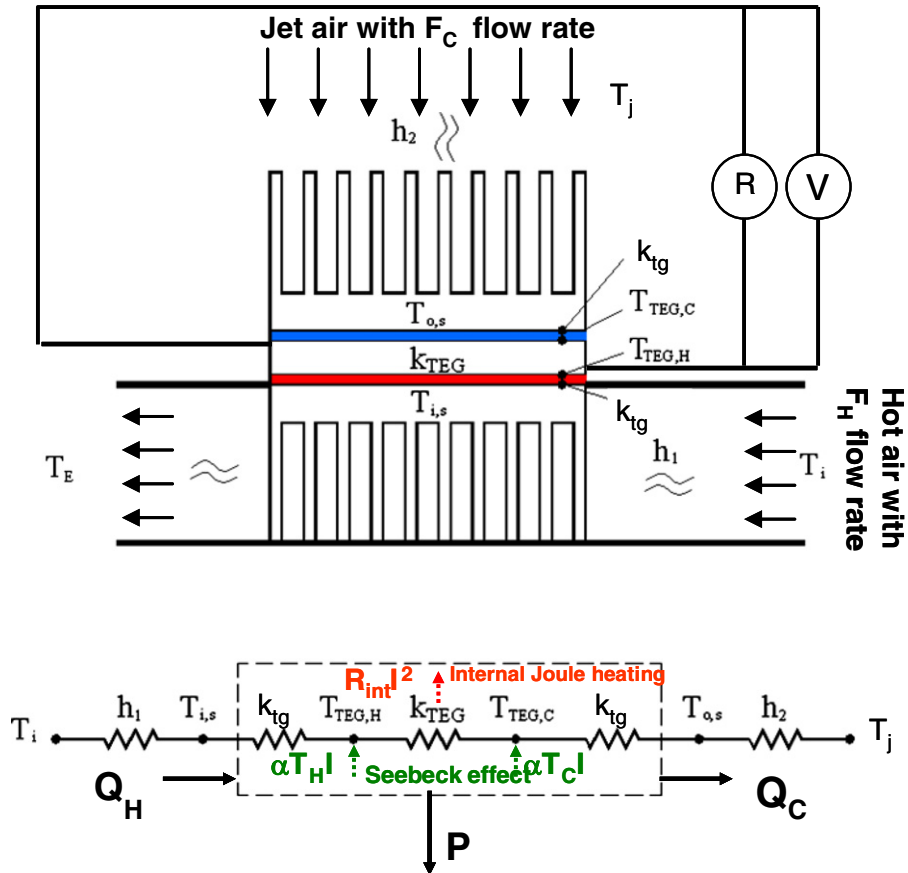


Fig. 3. Heat transfer mechanism and Seebeck effect for the present system.



$$T_{i,s} - T_{o,s} = \frac{(\gamma + \lambda + 1) \pm \sqrt{(\gamma + \lambda + 1)^2 - 4\alpha^* \lambda (T_i - T_j)}}{2\alpha^*}. \quad (16)$$

However,  $(T_{i,s} - T_{o,s})$  should increase with  $(T_i - T_j)$ . So only one reasonable solution of  $(T_{i,s} - T_{o,s})$  exists in Eq. (16), and it is

$$T_{i,s} - T_{o,s} = \frac{(\gamma + \lambda + 1) - \sqrt{(\gamma + \lambda + 1)^2 - 4\alpha^* \lambda (T_i - T_j)}}{2\alpha^*}. \quad (17)$$

Finally, the maximum generating electricity can be expressed as

$$P_{\max} = \frac{k_{\text{TEG}} A_{\text{TEG}}}{\delta} \cdot \frac{\left( (\gamma + \lambda + 1) - \sqrt{(\gamma + \lambda + 1)^2 - 4\alpha^* \lambda (T_i - T_j)} \right)^2}{4\alpha^*}. \quad (18)$$

### 2.3. Measurement of maximum generating electricity of thermoelectric conversion system

The maximum power of thermoelectric generator was measured according to the maximum power transfer theorem. If a voltage source is to transmit the maximum power to the load end, the electrical resistance of load end must be equal to the internal impedance of voltage source. Therefore, the output end of thermoelectric generator was connected to a variable-resistance load system, so as to adjust the ohm value of the variable resistance. The output voltage values under different loads were recorded and the generating electricity was calculated. The maximum value of the generating electricity resulted at the condition that the ohm value of the resistance ( $R$ ) of the external load meets that ( $R_{\text{int}}$ ) of the thermoelectric generators. In all the present tests, the ohm value of the resistance of the external load was set to obtain the maximum value of the generating electricity.

Fig. 4 shows the relation of the temperature difference  $(T_{i,s} - T_{o,s})$  between cold and hot sides of thermoelectric generators to the generating electricity ( $P$ ) for all the present experiments. It is observed that the generating electricity ( $P$ ) increases with the temperature difference  $(T_{i,s} - T_{o,s})$ . It meets the Seebeck effect. According to all experimental

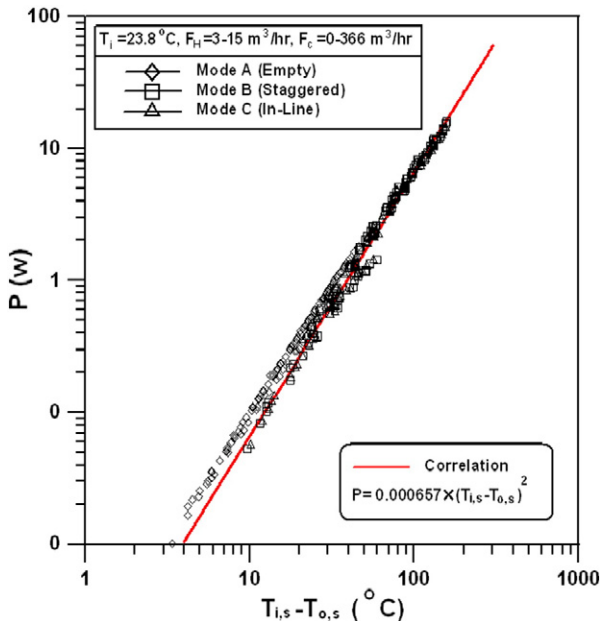


Fig. 4. Generating electricity ( $P$ ) as a function of temperature difference  $(T_{i,s} - T_{o,s})$ .

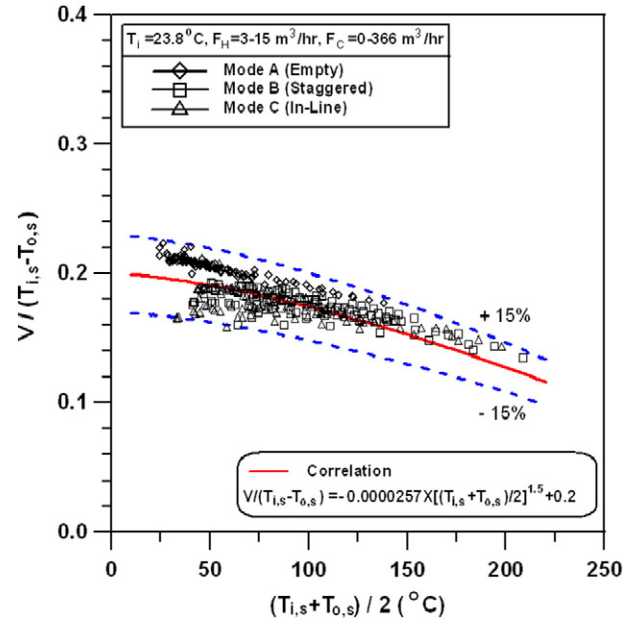


Fig. 5. Relationship between  $V / (T_{i,s} - T_{o,s})$  and mean temperature  $(T_{i,s} + T_{o,s}) / 2$  of TEGs.

data of four thermoelectric generators in series connection herein, an empirical formula of the generating electricity ( $P$ ) can be expressed as:

$$P = \frac{\alpha^2}{4R_{\text{int}}} (T_{i,s} - T_{o,s})^2 = 0.000657 \times (T_{i,s} - T_{o,s})^2 \quad (19)$$

Fig. 5 shows the relation between the mean temperature  $((T_{i,s} + T_{o,s}) / 2)$  of thermoelectric generators and  $V / (T_{i,s} - T_{o,s})$  for all the present experiments. It is observed that the  $V / (T_{i,s} - T_{o,s})$  (i.e. half of Seebeck coefficient difference  $(\alpha / 2)$  of thermoelectric generators) decreases as the mean temperature  $(T_{i,s} + T_{o,s}) / 2$  rises. This study concluded the empirical formula of the Seebeck coefficient difference of four thermoelectric generators in series connection as follows:

$$V / (T_{i,s} - T_{o,s}) = \alpha / 2 = -0.0000257 \times \left[ (T_{i,s} + T_{o,s}) / 2 \right]^{1.5} + 0.2. \quad (20)$$

Table 2

Properties of TEGs, heat absorber and heat sink in operation conditions.

Properties of 4 pieces of TEGs:

$$A_{\text{TEG}} = 0.0064 \text{ m}^2$$

$$\delta = 0.0038 \text{ m (including the ceramic base plates)}$$

$$k_{\text{TEG}} = 1.60 \text{ W/m/K (considering the ceramic base plates and TEG materials)}$$

$$R_{\text{int}} = 41.6 \Omega$$

$$(k_{\text{TEG}} \cdot A_{\text{TEG}}) / \delta = 2.695 \text{ W/K}$$

$$\alpha = (\alpha_p - \alpha_n) \approx 0.349 \text{ V/K (Eqs. (19) and (20))}$$

$$\alpha^* = \alpha^2 \cdot \delta / (4k_{\text{TEG}} \cdot A_{\text{TEG}} \cdot R_{\text{int}}) = 0.000272 \text{ K}^{-1}$$

Properties for operation conditions of heat absorber and heat sink:

$$F_H = 3-15 \text{ m}^3/\text{h (about the 4-stroke and single-cylinder engine with 125 c.c. displacement volume working at 5000 rpm)}$$

$$F_C = 122-366 \text{ m}^3/\text{h (about 30-80 km/h speed of the vehicle)}$$

$$(h_1 \cdot A_1)_B / A_{\text{TEG}} = 115 \cdot F_H^{0.618} \text{ W/m}^2/\text{K (measured herein by using the similar method in [13])}$$

$$(h_1 \cdot A_1)_C / A_{\text{TEG}} = 85.5 \cdot F_H^{0.611} \text{ W/m}^2/\text{K (measured herein by using the similar method in [13])}$$

$$(h_2 \cdot A_2) / A_{\text{TEG}} = 244 \cdot F_C^{0.219} \text{ W/m}^2/\text{K (measured herein by using the similar method in [14])}$$

$$\gamma_B = (h_1 \cdot A_1)_B / (h_2 \cdot A_2) = 0.471 \cdot F_H^{0.618} / F_C^{0.219}$$

$$\gamma_C = (h_1 \cdot A_1)_C / (h_2 \cdot A_2) = 0.350 \cdot F_H^{0.611} / F_C^{0.219}$$

$$\lambda_B = (h_1 \cdot A_1)_B \cdot \delta / (k_{\text{TEG}} \cdot A_{\text{TEG}}) = 0.273 \cdot F_H^{0.618}$$

$$\lambda_C = (h_1 \cdot A_1)_C \cdot \delta / (k_{\text{TEG}} \cdot A_{\text{TEG}}) = 0.203 \cdot F_H^{0.611}$$

### 3. Results and discussion

The variable parameters include: the inlet hot air temperature ( $T_i$ ); the hot air flow rate ( $F_H$ ); and the cooling air flow rate ( $F_C$ ). Controlling ( $T_i$ ) represents different setting positions of thermoelectric conversion system in real exhaust pipe of engine. The temperature of the exhaust is above 600 °C at the engine exhaust valve. When the exhaust has passed through the exhaust pipe, catalytic converter and silencer to the exhaust pipe outlet, the temperature of the exhaust has been lower than 100 °C. Controlling hot air flow rate ( $F_H$ ) means real vehicles have different discharge capacities at different rotational speeds of the engine; controlling cooling air flow rate ( $F_C$ ) represents leading in different external cooling effects. Table 2 shows the properties of 4 pieces of thermoelectric generators as well as the properties for operation conditions of heat absorber and heat sink, which are needed as using Eq. (19) to predict the generating electricity ( $P$ ).

Fig. 6 shows the influence of hot air inlet temperature ( $T_i$ ) on the generating electricity ( $P$ ) when  $F_H = 15 \text{ m}^3/\text{h}$ ,  $F_C = 366 \text{ m}^3/\text{h}$ . Fig. 7 shows the influence of hot air flow rate ( $F_H$ ) on the generating electricity ( $P$ ) when  $F_C = 366 \text{ m}^3/\text{h}$ ,  $T_i = 350 \text{ °C}$ , while Fig. 8 shows the effect of cooling air flow rate ( $F_C$ ) on the generating electricity ( $P$ ) when  $F_H = 15 \text{ m}^3/\text{h}$ ,  $T_i = 250 \text{ °C}$ . It is observed that the generating electricity ( $P$ ) increases with the hot air inlet temperature ( $T_i$ ), the hot air flow rate ( $F_H$ ) and the cooling air flow rate ( $F_C$ ) since higher ( $T_i$ ;  $F_H$ ;  $F_C$ ) would increase the temperature difference between the hot and cold sides of TEG. Besides, the generating electricity ( $P$ ) of the system with the staggered pin-fin heat absorber is somewhat higher than that with the in-line pin-fin one. It should be because the staggered pin-fin array has the higher heat transfer capacity [13] to make a higher temperature at the hot side of TEG. Figs. 6–8 also show the generating electricity ( $P$ ) of the system without heat absorber for comparison. It is observed that the generating electricity ( $P$ ) of the system with heat absorber is far larger than that without heat absorber, suggesting the important influence of heat absorber on the generating electricity ( $P$ ). Finally, the predicted values of the generating electricity ( $P$ ) by using Eq. (19) are also plotted in Figs. 6–8. They generally agree with the experimental data, demonstrate the validity of the proposed theoretical model.

Figs. 9–11 show the effects of some critical thermal parameters, such as  $\gamma$ ,  $\lambda$  and  $\alpha^*$  defined in Eq. (14), on the generating electricity ( $P$ ). The  $\gamma$ ,  $\lambda$  and  $\alpha^*$  represent respectively the heat-transfer ratio of heat absorber to heat sink, the Biot number and the Seebeck parameter of the

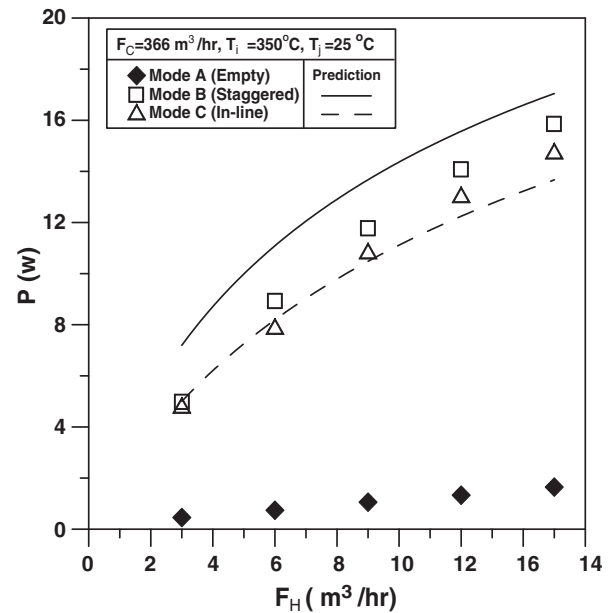


Fig. 7. Effect of  $F_H$  on generating electricity ( $P$ ) for various heat absorbers.

thermoelectric generator. All the values of the generating electricity ( $P$ ) plotted in Figs. 9–11 are predicted by using Eq. (19). Fig. 9 depicts the influence of  $\gamma$  on the generating electricity ( $P$ ) for various ( $T_i - T_j$ ) at specified values of  $\lambda$ ,  $\alpha^*$  and  $k_{TEG}A_{TEG} / \delta$ . It can be found that, at specified values of  $\lambda$ ,  $\alpha^*$ ,  $k_{TEG}A_{TEG} / \delta$  and ( $T_i - T_j$ ), there is a limit value of the generating electricity ( $P$ ) as  $\gamma$  approaching zero. When the value of  $\gamma$  increases, the generating electricity ( $P$ ) firstly decreases with  $\gamma$  slowly till  $\gamma$  is around 0.1 and then drops sharply for the present cases. It means that there is a critical value of  $\gamma$ , which is also an economic design for heat absorber and heat sink at specified operation conditions, to have the almost maximum generating electricity. Fig. 10 displays the effect of  $\lambda$  on the generating electricity ( $P$ ) for various  $\gamma$  at specified values of ( $T_i - T_j$ ),  $\alpha^*$  and  $k_{TEG}A_{TEG} / \delta$ . The predicted data indicates that, at the present values of ( $T_i - T_j$ ),  $\alpha^*$  and  $k_{TEG}A_{TEG} / \delta$ , there exists a limit value of the generating electricity ( $P$ ) as  $\lambda$  approaching infinite for various values of  $\gamma$ . Besides, the generating electricity ( $P$ ) firstly increases

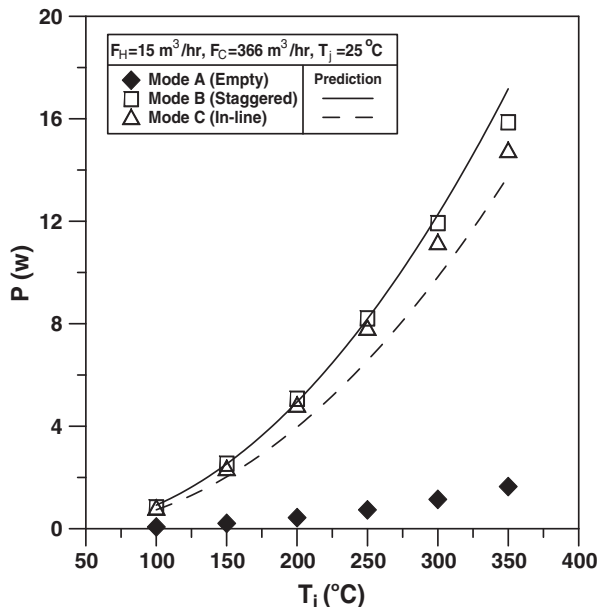


Fig. 6. Effect of  $T_i$  on generating electricity ( $P$ ) for various heat absorbers.

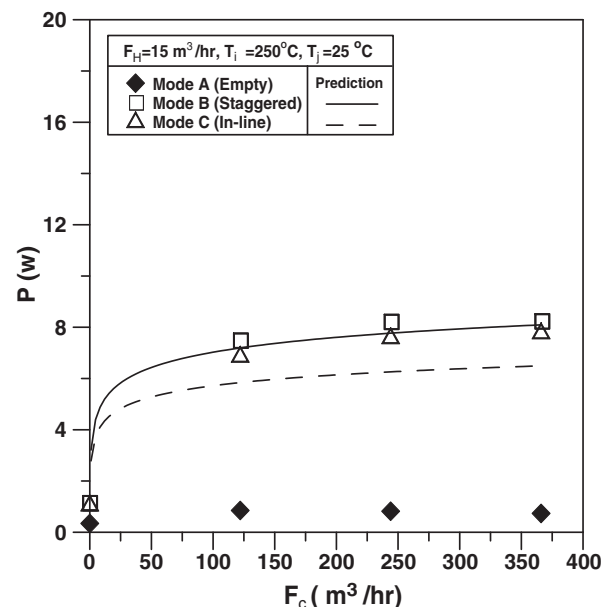


Fig. 8. Effect of  $F_C$  on generating electricity ( $P$ ) for various heat absorbers.

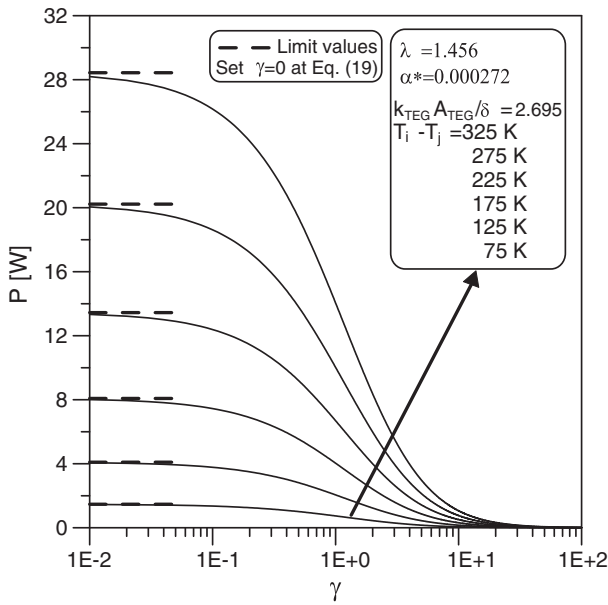


Fig. 9. Effect of  $\gamma$  on generating electricity ( $P$ ) for various  $(T_i - T_j)$ .

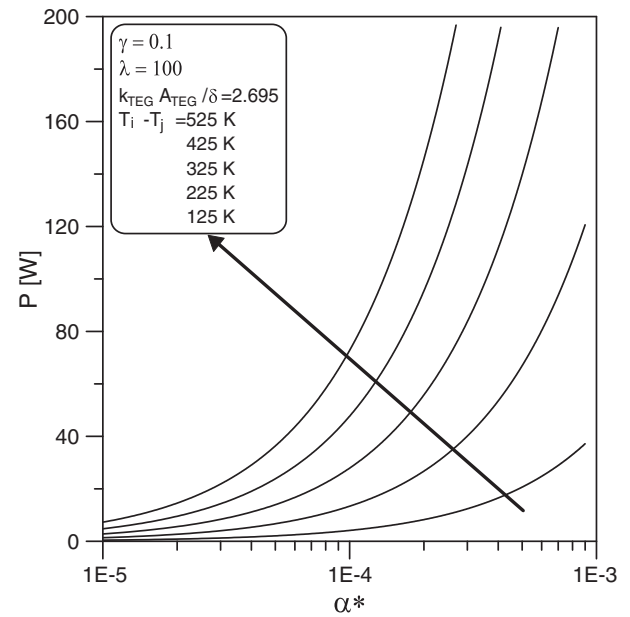


Fig. 11. Effect of  $\alpha^*$  on generating electricity ( $P$ ) for various  $(T_i - T_j)$ .

with  $\lambda$  and then approaches to a limit value as  $\lambda$  is about 100 for the present cases. Therefore, it may have a critical value of  $\lambda$  (i.e. the Biot number of the thermoelectric generator), which is also an economic design for heat absorber at specified operation conditions, to have the almost maximum generating electricity. Finally, Fig. 11 represents the influence of  $\alpha^*$  on the generating electricity ( $P$ ) for various  $(T_i - T_j)$  at specified values of  $\lambda$ ,  $\gamma$  and  $k_{TEG} A_{TEG} / \delta$ . The generating electricity ( $P$ ) increases with the Seebeck parameter ( $\alpha^*$ ) monotonically. It meets the Seebeck effect.

#### 4. Conclusions

This study developed an integral thermoelectric generator system with high-performance heat transfer and thermoelectric conversion function, using the metal pin-fin array coupling with the forced convection heat transfer technique to be the heat absorber and heat sink. A

series of systematical experiments were performed successfully to obtain the generating electricity of an integral thermoelectric generator system working at the exhaust pipe for various operation conditions, including (1) the configuration of the heat absorber; (2) the inlet temperature of hot air ( $T_i = 100\text{--}350\text{ }^\circ\text{C}$ ); (3) the flow rate of hot air ( $F_H = 3\text{--}15\text{ m}^3/\text{h}$ ) and (4) the flow rate of cooling air ( $F_C = 0\text{--}366\text{ m}^3/\text{h}$ ). A one-dimensional steady heat conduction model with internal Joule heat generation and Seebeck effect was also proposed. The experimental results demonstrated the validity of the proposed theoretical model. Finally, some critical heat-transfer parameters on the generating electricity of the integral thermoelectric generator system were provided and discussed to be reference for next physical product design.

#### Acknowledgments

The authors would like to thank the National Science Council of the Republic of China for financially supporting this research under Contract Nos. NSC 100-2221-E-270-014-MY3, NSC-100-2632-E-270-001-MY3 and NSC-97-2221-E-344-003.

#### References

- [1] H.L. Talom, A. Beyene, Heat recovery from automotive engine, *Appl. Therm. Eng.* 29 (2009) 439–444.
- [2] D.M. Rowe, Thermoelectrics an environmentally-friendly source of electrical power, *Renew. Energy* 16 (1999) 1251–1256.
- [3] T.J. Hendricks, J.A. Lustbader, Advanced thermoelectric power system investigations for light-duty and heavy-duty applications, *Proceedings of the 21st international conference on thermoelectrics*, Long Beach, CA, 2002.
- [4] A.K. Pramanick, P.K. Das, Constructural design of a thermoelectric device, *Int. J. Heat Mass Transf.* 49 (2006) 1420–1429.
- [5] S. Lineykin, S. Ben-Yaakov, Modeling and analysis of thermoelectric modules, *IEEE Trans. Ind. Appl.* 43 (2007) 505–512.
- [6] G. Fraisse, M. Lazard, C. Goupil, J.Y. Serrat, Study of a thermoelement's behavior through a modeling based on electrical analogy, *Int. Commun. Heat Mass Transfer* 53 (2010) 3503–3512.
- [7] H.-S. Huang, Y.-C. Weng, Y.-W. Chang, S.-L. Chen, M.-T. Ke, Thermoelectric water-cooling device applied to electronic equipment, *Int. Commun. Heat Mass Transfer* 37 (2010) 140–146.
- [8] C. Junior, G. Chen, J. Koehler, Modeling of a new recuperative thermoelectric cycle for a tumble dryer, *Int. J. Heat Mass Transf.* 55 (2012) 1536–1543.
- [9] M. Chen, L.A. Rosendahl, T. Condra, A three-dimensional numerical model of thermoelectric generators in fluid power systems, *Int. J. Heat Mass Transf.* 54 (2011) 345–355.
- [10] E.J. Sandoz-Rosado, S.J. Weinstein, R.J. Stevens, On the Thomson effect in thermoelectric power devices, *Int. J. Therm. Sci.* (2012), <http://dx.doi.org/10.1016/j.ijthermalsci.2012.10.018>.

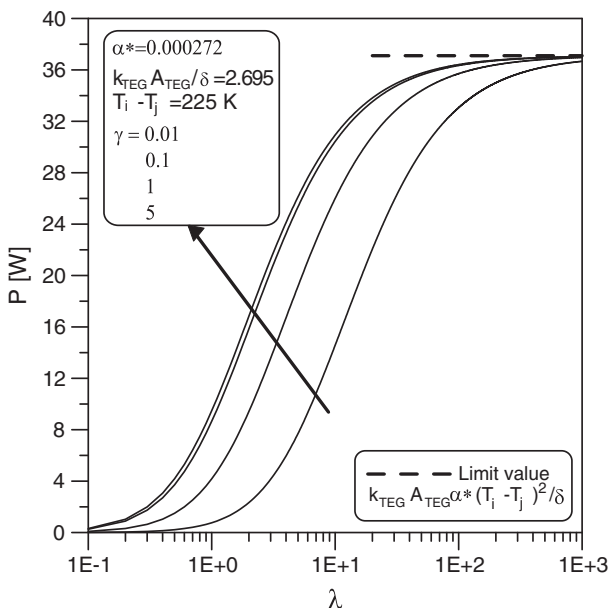


Fig. 10. Effect of  $\lambda$  on generating electricity ( $P$ ) for various  $\gamma$ .



- [11] A. Rezaei, L.A. Rosendahl, S.J. Andreasen, Experimental investigation of thermoelectric power generation versus coolant pumping power in a microchannel heat sink, *Int. Commun. Heat Mass Transfer* 39 (2012) 1054–1058.
- [12] T.M. Jeng, S.C. Tzeng, Pressure drop and heat transfer of square pin-fin arrays in in-line and staggered arrangements, *Int. J. Heat Mass Transf.* 50 (2007) 2364–2375.
- [13] T.M. Jeng, A porous model for the square pin-fin heat sink situated in a rectangular channel with laminar side-bypass flow, *Int. J. Heat Mass Transf.* 51 (2008) 2214–2226.
- [14] T.M. Jeng, S.C. Tzeng, H.J. Liao, Flow visualizations and heat transfer measurements for a rotating pin-fin heat sink with a circular impinging jet, *Int. J. Heat Mass Transf.* 52 (2009) 2119–2131.